Signatures of non-Markovianity in cavity QED with color centers in two-dimensional materials

Svendsen, Mark Kamper; Ali, Sajid; Stenger, Nicolas; Thygesen, Kristian Sommer; Iles-Smith, Jake

Published in:
Physical Review Research

Link to article, DOI:
10.1103/PhysRevResearch.5.L032037

Publication date:
2023

Document Version
Publisher's PDF, also known as Version of record

Letter

Signatures of non-Markovianity in cavity QED with color centers in two-dimensional materials

Mark Kamper Svendsen,[1] Sajid Ali,[1,2] Nicolas Stenger,[3,4,5] Kristian Sommer Thygesen,[1,4] and Jake Iles-Smith[6,7,*]

[1]*CAMD, Department of Physics, Technical University of Denmark, 2800 Kongens Lyngby, Denmark*
[2]*School of Physics and Astronomy, Monash University, Victoria 3800, Australia*
[3]*Department of electrical and photonics engineering, Technical University of Denmark, 2800 Kongens Lyngby, Denmark*
[4]*Center for Nanostructured Graphene, Technical University of Denmark, 2800 Kongens Lyngby, Denmark*
[5]*NanoPhoton–Center for Nanophotonics, Technical University of Denmark, 2800 Kongens Lyngby, Denmark*
[6]*Department of Physics and Astronomy, The University of Manchester, Oxford Road, Manchester M13 9PL, United Kingdom*
[7]*Department of Electrical and Electronic Engineering, The University of Manchester, Oxford Road, Manchester M13 9PL, United Kingdom*

(Received 2 August 2022; revised 30 March 2023; accepted 15 May 2023; published 15 September 2023)

Light-matter interactions of defects in two-dimensional materials are expected to be profoundly impacted by strong coupling to phonons. In this work, we combine *ab initio* calculations of a defect in hBN with a fully quantum mechanical and numerically exact description of a cavity-defect system to elucidate this impact. We show that, even at weak light-matter coupling, the dynamical evolution of the cavity-defect system has clear signatures of non-Markovian phonon effects, and that linear absorption spectra show the emergence of hybridized light-matter-phonon states in regimes of strong light-matter coupling. We emphasise that our methodology is general, and can be applied to a wide variety of material-defect systems.

DOI: 10.1103/PhysRevResearch.5.L032037

Single-photon emission has been observed from a broad range of two-dimensional materials (2DM) [1–7]. Of particular interest to quantum technologies is emission from defect complexes in hexagonal boron nitride (hBN) [8–13], owing to the material's wide band gap [14] and stability of the emitters [10,15]. Not only does the precise nature of these defect complexes remain under scrutiny [10,11,16], but also their quantum optical properties remain largely unexplored, particularly in strong light-matter coupling regimes [17,18]. Crucially, the optical properties of condensed matter systems cannot be understood through standard quantum optics theory, since strong system-environment interactions lead to a breakdown of the underpinning perturbative methods [19,20]. Of particular relevance to the optical properties of defect complexes in 2DM are strong electron-phonon interactions. Specifically, defect emission spectra typically show sharp and well resolved phonon sidebands [21–24], a hallmark of vibronic state formation and long lived electron-phonon correlations. It is therefore crucial that any theory describing the dynamical or optical behavior of a 2DM defect complex accurately accounts for electron-phonon interactions.

To this end, we study the cavity quantum electrodynamics (cQED) of defects in 2DM [17,18], focusing on two color centers in hBN proposed as single-photon emitters, the C_BV_N [10,25] and C_2C_N defect complexes [26,27]. We accurately account for electron-phonon interactions by combining *ab initio* calculations with a fully quantum mechanical and numerically exact description of the dynamics of the defect states interacting with a single mode optical cavity. The former provides an atomistic description of the phonon modes of the material system. The latter employs the time evolved matrix product operator (TEMPO) algorithm [28], where non-Markovian influences of the phonon environment are encoded within a tensor network. When combined with tensor compression methods, TEMPO provides an efficient approach for calculating the reduced dynamics of the system [29–31], which we extend to extract the linear response spectrum of the defect-cavity system. This hybrid approach is inspired by [32] and allows us to maintain the accuracy and insight of first-principles calculations, while enabling coherent dynamics to be captured in regimes of light-matter coupling inaccessible to first-principles methods.

A central finding of this work is that electron-phonon interactions in the studied defect complexes lead to highly non-Markovian dynamics, even in regimes of moderate light-matter coupling strengths accessible to state-of-the-art experiments. We attribute this behavior to coherent coupling between the defects electronic states and high-quality (Q) factor phonon modes, where the lifetime of the phonon mode becomes comparable to the Rabi oscillations in the photonic degrees of freedom, and thus tripartite coherent oscillations emerge. This provides a mechanism to optically manipulate mechanical modes of a condensed matter system that would otherwise not directly couple to light. Furthermore, from linear response spectra, we see evidence of hybridization between cavity-defect polaritons and high-Q phonon modes when entering regimes of strong light-matter coupling. These states bear resemblance to recently predicted exciton-photon-phonon hybridization in hBN [33]; however, in this instance

*jake.iles-smith@manchester.ac.uk

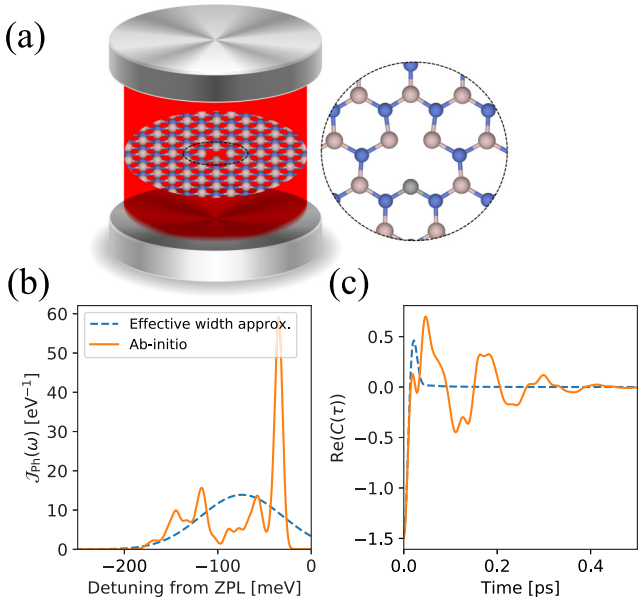

FIG. 1. (a) A schematic figure of the C_BV_N defect in hBN interacting with a single quantized field mode. This mode could be plasmonic or photonic in nature. (b) A plot of the *ab initio* (solid) and effective width (dashed) spectral densities. Using the atomistic simulation, we ascribe the dominant peak at ∼125 meV to a phonon breathing mode. (c) The bath correlation function for the *ab initio* (solid) and effective width (dashed) spectral densities. The sharp peaks of the *ab initio* spectral density leads to long lived oscillations in the correlation function, which are washed out when an effective width approximation is used.

they occur in a continuum of modes coupled to a defect state, and therefore will inherit nonlinear features from the localized electronic states. For simplicity we focus on the C_BV_N defect complex in this Letter, leaving the discussion of C_2C_N to the Supplemental Material (SM) [34]. The electronic structure of the C_BV_N defect consists of two manifolds [35]: the first consists of the $(2)^1A_1$ and $(1)^1B_1$ excited states and a $(1)^1A_1$ singlet ground state; the second contains the triplet states $(1)^3B_1$ and $(2)^3B_1$ [16], separated in energy by $\hbar\omega_e = 2$ eV [35]. By assuming that the intersystem crossing due to spin-orbit coupling occurs on a much longer timescale (10–100 ns) than cavity-enhanced optical transitions (<1 ns), we restrict our attention to the triplet state manifold, which reduces to a two-level system with ground and exited states $|g\rangle$ and $|e\rangle$ respectively [36]. We assume that the electronic transition interacts with an electromagnetic environment through two pathways: either through the modes of an optical cavity [as shown schematically in Fig. 1(a)] or through leakage to background modes.

The single mode cavity has a resonant frequency $\hbar\Omega_c$ and cavity width κ. This may be described by the Jaynes-Cummings interaction [37,38]:

$$H_S = \hbar\omega_e\sigma^\dagger\sigma + \hbar g(\sigma^\dagger a + \sigma a^\dagger) + \hbar\Omega_c a^\dagger a, \qquad (1)$$

where $\sigma = |g\rangle\langle e|$ is the dipole transition operator, a ($a^\dagger$) is the annihilation (creation) operator of the cavity mode, and $\hbar g$ is the coupling strength between the emitter and the cavity. The cavity loss is included in the evolution of the system in terms of the Lindblad dissipator $\kappa L_a\rho$, where $L_o\rho = o\rho o^\dagger - \{o^\dagger o, \rho\}/2$ [37]. Here we limit ourselves to the single excitation subspace, spanned by the basis $\{|g,0\rangle, |e,0\rangle, |g,1\rangle\}$.

An emitter coupled to an optical cavity will also couple to a background electromagnetic environment, where photons are emitted directly into free-space electromagnetic modes rather than via the cavity [39]. We account for this by introducing a second electromagnetic environment that couples to the electronic transition, in the rotating wave approximation this interaction takes the form $H_I^{EM} = \sum_{\mathbf{l}}(\hbar f_{\mathbf{l}}\hat{\sigma}^\dagger c_{\mathbf{l}} + \text{H.c.})$, where $c_{\mathbf{l}}$ is the annihilation operator for the $\mathbf{l}$th mode of the background electromagnetic environment. We assume that the interaction between the emitter and the background field is weak and strictly Markovian, where the coupling to the field does not vary appreciably over frequencies relevant to the emitter. This allows us to make the white noise approximation in which the background electromagnetic environment is δ correlated with the emitter [40]. This is equivalent to assuming $f_{\mathbf{l}} = \sqrt{2\pi\Gamma}$ [40,41], where Γ is the background spontaneous emission rate. With the above approximations and tracing over the external EM fields, the optical contribution to the system evolution is determined through the superoperator $\mathcal{V}_t = \exp(t\,\mathcal{L}_S)$, where $\mathcal{L}_S\rho = -i[H_S, \rho] + \Gamma L_\sigma\rho + \kappa L_a\rho$. For a full derivation and discussion please refer to the SM [34].

We take a linear electron-phonon interaction [42] of the form $H_I^{Ph} = \sigma^\dagger\sigma\sum_{\mathbf{k}}\hbar g_{\mathbf{k}}(b_{\mathbf{k}}^\dagger + b_{-\mathbf{k}})$, where $b_{\mathbf{k}}$ is the annihilation operator for a phonon mode with wave vector $\mathbf{k}$, with free field evolution $H_B^{Ph} = \sum_{\mathbf{k}}\hbar\omega_{\mathbf{k}}b_{\mathbf{k}}^\dagger b_{\mathbf{k}}$, and $g_{\mathbf{k}}$ is the electron-phonon coupling strength of the $\mathbf{k}$th phonon mode. The electron-phonon coupling is fully characterised by the spectral density $\mathcal{J}_{Ph}(\omega) = \sum_{\mathbf{k}} S_{\mathbf{k}}\delta(\omega - \omega_{\mathbf{k}})$, where $S_{\mathbf{k}} = \omega_{\mathbf{k}}^{-2}|g_{\mathbf{k}}|^2$ is the partial Huang-Rhys factor of mode $\mathbf{k}$. The total Huang-Rhys parameter is recovered by integrating the spectral density $S_{Tot} = \int_0^\infty d\omega\mathcal{J}_{Ph}(\omega)$.

To determine the partial Huang-Rhys factors, and therefore the spectral density, we treat the electron-phonon coupling from first principles, using density functional theory (DFT) to calculate the normal modes of the ground and excited states of the hBN lattice with the considered defect complex. Importantly, differences in the ground and excited state electronic configuration may alter the normal modes of the system in both frequency and spatial direction. We account for these differences when calculating the partial Huang-Rhys factors using the method outlined by Duschinsky [43], where geometric differences in the normal modes are accounted for using an affine coordinate transformation [44]. The DFT calculations of the phonons were performed for periodically repeated defect complexes in hBN monolayers using the Vienna Ab Initio Simulation Package (VASP) [45]. The exact details of the DFT calculations are given in the SM [34].

The resulting spectral density is shown in Fig. 1(b), where we see multiple sharp peaks present. These peaks correspond to high-Q phonon modes present in hBN; notably from the atomistic simulations we can assign the dominant contributions to the peak ∼125 meV from delocalized defect breathing modes, in which the atoms surrounding the defect oscillate along the dipole direction of the defect.

To understand the influence of these modes will have on the cavity-defect system, we calculate the bath correlation

function

$$C(\tau) = \int_0^\infty d\omega\, \mathcal{J}_{\rm Ph}(\omega)[\cos(\omega\tau)\coth(\omega/2k_{\rm B}T) - i\sin(\omega\tau)],$$

shown in Fig. 1(c), where T is the temperature, $k_{\rm B}$ is the Boltzmann constant, and we have assumed the phonon bath to be initially in thermal equilibrium. This correlation function encodes the timescales over which memory effects last between the system and environment [46], see the SM [34] for details. The sharp peaks in the *ab initio* spectral density induce long lived oscillation in the correlation function, which are attributed to high-Q phonon modes. To highlight the importance of this structure we can replace the spectral density with a broadened function with the same total Huang-Rhys parameter, as shown by the dashed curve in Fig. 1(b). The corresponding correlation function, shown in Fig. 1(c), has only small rapidly damped oscillations.

To study the time evolution of the composite cavity-emitter system, we employ the time-evolving matrix product operator (TEMPO) algorithm initially developed by Strathearn *et al.* [28]. TEMPO is a powerful method for the study of open quantum systems in strong coupling regimes [29,30], and has been applied to quantum thermodynamics in the strong coupling regime [47], as well as nonadditive phenomena [31], and optimal control [48]. The starting point for the TEMPO formalism, alongside other numerically exact path integral methods [49–51], is the Trotter decomposition [52], where for a sufficiently small time increment δt the propagator for the open system can be factorized as $\mathcal{U}_{\delta t} = e^{(\mathcal{L}_S+\mathcal{L}_B)\delta t} \approx \mathcal{V}_{\delta t}^{1/2}\mathcal{W}_{\delta t}\mathcal{V}_{\delta t}^{1/2} + \mathcal{O}(\delta t^3)$. The superoperator $\mathcal{V}_{\delta t}$ is as defined above, and captures the evolution of the system and dissipation through the external electromagnetic fields. The system-phonon interaction is captured through $\mathcal{W}_{\delta t} = \exp(\delta t\mathcal{L}_{\rm B})$, and is given by $\mathcal{L}_{\rm B}\rho = -i[H_{\rm I}^{\rm Ph} + H_{\rm B}^{\rm Ph}, \rho]$.

This partitioning allows one to construct a discrete-time influence functional of Feynman-Vernon type [49,50], capturing the influence of the environment to all orders in the interaction strength. The reduced state after k time steps is

$$\rho^{\alpha_k} = \sum_{\vec{\alpha},\vec{\beta}} \rho^{\alpha_0} \prod_{j=1}^{k} \mathcal{V}_{\beta_j}^{\alpha_j}\mathcal{V}_{\alpha_{j-1}}^{\beta_j}\mathcal{F}_{\beta_k\cdots\beta_1}, \tag{2}$$

where we have introduced the compound indices $\alpha_k = (s_k, r_k)$ and $\beta_k = (t_k, u_k)$, such that $\rho^{\alpha_k} = \langle r_k|\rho|s_k\rangle$, and $\mathcal{V}_{\beta_k}^{\alpha_k} = \langle r_k|\mathcal{V}_{\delta t}[|t_k\rangle\langle u_k|]|s_k\rangle$. The influence of the phonon environment is captured by the influence tensor $\mathcal{F}_{\beta_k\cdots\beta_1} = {\rm tr}_E(\mathcal{W}^{\beta_k}\cdots\mathcal{W}^{\beta_1}[\tau_B])$, where $\mathcal{W}^{\beta_k} = \langle t_k|\mathcal{W}_{\delta t}[|t_k\rangle\langle u_k|]|u_k\rangle$. By taking the initial state of the environment to be in thermal equilibrium,

$$\tau_B = \exp\left(-\sum_k \nu_k b_k^\dagger b_k/k_BT\right)\Big/ {\rm tr} \times \left[\exp\left(-\sum_k \nu_k b_k^\dagger b_k/k_BT\right)\right],$$

the trace over the environmental degrees of freedom can be done analytically [49,50].

Crucially, the influence tensor scales exponentially in the number of time steps taken [49,50]; while applying a finite time memory approximation can reduce the computational cost of propagating the reduced state to long times [49,50,53], it limits one to scenarios where key dynamics occur on short timescales. A key insight of Strathearn *et al.* [28] was that the influence tensor may be represented in matrix product operator (MPO) form. This allows one to encode the exponentially growing tensor as a tensor network and apply tensor compression [54] to reduce the rank of each network element, circumventing exponential scaling. The reduced state of the system is then calculated by contracting the network down after each time step. The convergence of the TEMPO algorithm is sensitive to taking a sufficiently small time step δt, and the degree to which the tensors are compressed. Further details of TEMPO and its convergence properties are discussed in the SM [34].

We now consider the dynamics of the cavity-defect system initialized in the state $\rho(0) = |e,0\rangle\langle e,0|$. Figure 2 shows the time evolution of the excited state population and the cavity mode occupation for different cavity parameters. We find that across all parameter regimes TEMPO predicts complex oscillations in the cavity occupation. We attribute these oscillations to high-Q phonon modes in the environment, which lead to long lived oscillations in the bath correlation function shown in Fig. 1(c); indeed these oscillations follow closely those in the bath correlation function. We confirm this by repeating the TEMPO calculations with the effective width spectral density shown in Fig. 1(b). Since this spectral density has the same total Huang-Rhys parameter, naively we might expect similar dynamics. However, the resulting dynamics in Fig. 2 show no oscillations at weak light-matter coupling, suggesting it is indeed the structure in the spectral density that has the dominant contribution to non-Markovian behavior. Interestingly, phonon induced oscillations are present in the cavity dynamics across all parameter regimes studied, but only emerge in the emitter dynamics in the strong light-matter coupling regime. This is a consequence of phonon induced fluctuations of the defects' excited state energy; the cavity is sensitive to these fluctuations through the dipole coupling with the emitter, leading to the observed oscillations in the occupation. However, these effects do become increasingly visible in the emitter dynamics with increasing coupling strength, where coherent vacuum Rabi oscillations occur.

We now turn our attention to the linear spectrum of the cavity-defect system. The linear response of an electronic system coupled to a quantized mode can be formulated either as an external field coupling to the electronic degrees of freedom, or by an external current pumping the cavity mode [55,56]. In both cases the driving is included as a perturbation at the Hamiltonian level, such that $H'(t) = H + E(t)\cdot\mu$. Here the system transition operator can be $\mu = \{\sigma^\dagger + \sigma, a^\dagger + a\}$. The first is the dipole operator of the defect, describing the scattering of light directly off the two level transition, and forms the basis of standard linear response theory [57]. The second is the quadrature operator of the cavity field, which induces a static polarization of the cavity mode and excites real photons into the field [56]. $E(t)$ then corresponds to the external field or the external current respectively. Treating the driving as weak, we can extract the linear response spectrum using density matrix perturbation theory [57]. Taking the semi-impulsive limit where $E(t) \propto e^{i\omega_D t}\delta(t)$, and ω_D is the

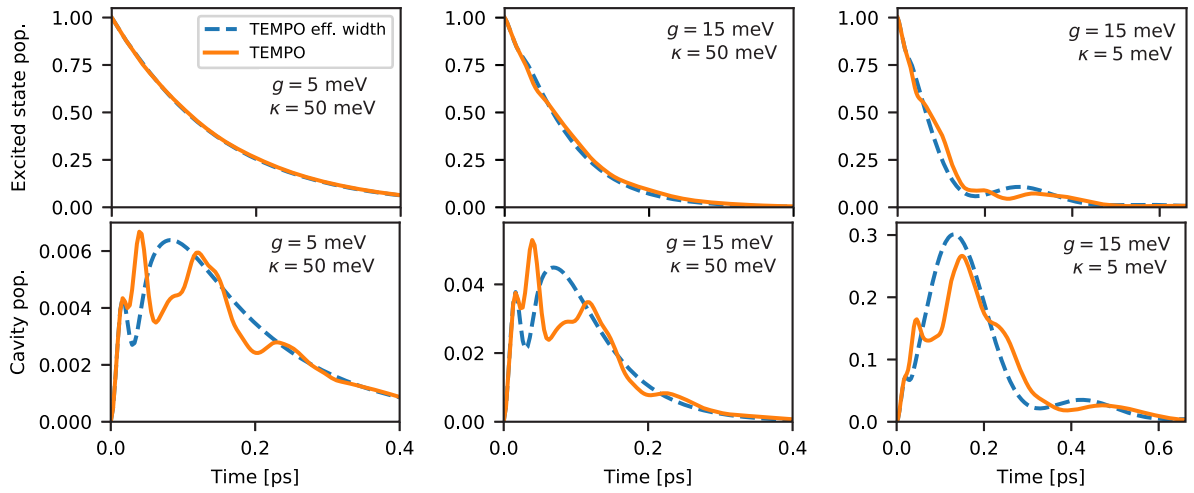

FIG. 2. Time dependent emitter population (top) and cavity occupation (bottom) for different coupling strengths and cavity widths. In contrast to the effective width spectral density (dashed), the *ab initio* spectral density (solid orange) predicts significant oscillations in the cavity occupation over all parameter regimes. Parameters used are $T = 4$ K, $\Gamma = 4$ meV, and $\hbar\Omega_c = \hbar\omega_e - \hbar\lambda$, where $\lambda = \int_0^\infty d\omega\, \omega^{-2} \mathcal{J}_{\rm Ph}(\omega)$ is the reorganization energy. The step size used to obtain convergence was $dt = 3.2$ fs, with SVD cutoff $\epsilon_{\rm C} = 10^{-6}$.

driving frequency, we obtain the absorption spectrum:

$$A(\omega) = 2\,\mathrm{Re}\left[\int_0^\infty dt\, e^{i\omega t} S^{(1)}(t)\right], \tag{3}$$

where $S^{(1)}(t) = \mathrm{tr}(\mu(t)[\mu(0), \chi(-\infty)])$ is the first-order response function. The global equilibrium density operator is $\chi(-\infty) = |g, 0\rangle\langle g, 0| \otimes \tau_B \otimes |\{0\}\rangle\langle\{0\}|$, where $|\{0\}\rangle$ denotes the vacuum state of the electromagnetic field. The above expressions allow us to extend TEMPO to calculate the first-order response function by propagating the initial system state $\rho(0) = \mu(0)|g, 0\rangle\langle g, 0|$.

Figures 3(a)–3(c) show the absorption spectra of the cavity mode when driven by an external current for various cavity parameters. To understand the role of phonons in these spectra, we artificially include a scaling parameter to spectral density $\mathcal{J}_{\rm Ph}(\omega) \to \alpha_{\rm HRF}\mathcal{J}_{\rm Ph}(\omega)$, where $\alpha_{\rm HRF} \in [0, 1]$, equivalent to scaling the total Huang-Rhys parameter. Figure 3(a) shows absorption spectrum at the onset of the strong coupling regime, where $g = \kappa$. In the absence of phonons ($\alpha_{\rm HRF} = 0$) we see a clear Rabi splitting, with the separation of the peaks determined by the the light-matter coupling g. As $\alpha_{\rm HRF}$ increases, the separation of these peaks is reduced. We can understand this reduction by appealing to the polaron formalism commonly used to study the behavior semiconductor quantum dots [20,58]: here, the light-matter coupling strength is reduced by the Franck-Condon factor $\mathscr{F} = \exp(-\alpha_{\rm HRF} S_{\rm Tot}/2)$, which accounts for the geometric difference of the phonon modes associated to the emitters ground and excited states. Figure 3(d) compares the peak separation as a function of the scaling parameter $\alpha_{\rm HRF}$ for the three parameter regimes. For the parameters associated with Fig. 3(a), the peak separation follows the Franck-Condon factor $\mathscr{F}$ (solid curve).

In regimes of stronger light-matter coupling shown in Figures 3(b) and 3(c), a more complex picture emerges: significant structure becomes apparent in the spectra as $\alpha_{\rm HRF}$ increases. Of particular interest is the departure from the well understood polaronic physics seen in Fig. 3(a), which is highlighted in Fig. 3(d). Here we see that at stronger coupling regimes ($g = 50$ meV), the renormalization no longer follows the Franck-Condon factor, and in the regime of strong light-matter coupling ($g = 100$ meV) we see the splitting increase with $\alpha_{\rm HRF}$. We attribute this behavior to a hybridization of the light-matter polariton and high-Q phonon modes. The resultant state is a tripartite quasiparticle with characteristics of light, matter, and vibrations. This can be seen most clearly in the upper polariton of Fig. 3(c), where an additional splitting emerges when $\alpha_{\rm HRF} \to 1$. This interpretation is supported

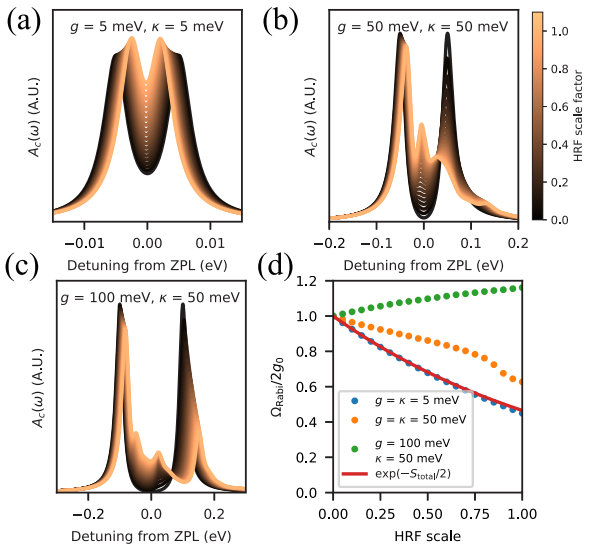

FIG. 3. (a)–(c) The linear absorption spectra when probing the cavity mode, for various values of the scaling parameter $\alpha_{\rm HRF}$. Here structure in the absorption spectra becomes increasingly important for large coupling, and broad cavity widths. (d) The change in peak position as a function of $\alpha_{\rm HRF}$ (points) for the cavity parameters studied in (a)–(c). All other parameters are the same as Fig. 2.

by the C_2C_N calculations shown in the SM [34]; this defect complex has a spectral density with little low energy structure, such that at $g = 50$ meV no hybridization occurs, and the renormalization of the Rabi frequency follows closely the Franck-Condon factor $\mathscr{F}$. It is only at higher light-matter coupling strengths ($g = 100$ meV) for C_2C_N, when the polariton splitting approaches resonance with a high-Q phonon mode that we observe a departure from Franck-Condon physics, heralding hybridised polariton-polaron states.

In this Letter we have combined atomistic simulations of a defect complex in hBN with TEMPO, a numerically exact and fully quantum mechanical simulation method. Our hybrid approach allows us to study realistic emitters beyond phenomenological and approximate treatments [22], providing a complete description of electron-phonon interactions in condensed matter emitters in optical or plasmonic cavities, with direct relevance to ongoing experiments. Furthermore, by considering the cavity quantum electrodynamics of a defect across the weak and strong light-matter coupling regimes, we have shown that strong coupling to high-Q vibrational modes play a significant role in determining the dynamics of the cavity-defect system, even in the weak light-matter coupling regime. At strong light-matter coupling, the absorption spectrum show clear signatures of hybridization between the light-matter polaritons and phonon modes inherent to hBN.

The method we present here is general, and not restricted to the material system or specific defect complexes studied here, with potential application to organic polaritons [59]. It is worth noting that we have restricted ourselves to low temperatures in the above discussion; at elevated temperatures phonon processes beyond linear electron-phonon coupling become important through mechanisms such as the Jahn-Teller effect [60].

We thank Mortiz Fischer and Emil V. Denning for insightful conversations. The work is supported by the BIOMAG project funded by the Novo Nordisk Foundation (Grant No. NNF21OC0066526). We also acknowledge funding from the European Research Council (ERC) under the European Unions Horizon 2020 research and innovation program Grant No. 773122 (LIMA). K.S.T. is a Villum Investigator supported by Villum Foundation (Grant No. 37789). This work was supported by the Danish National Research Foundation through NanoPhoton–Center for Nanophotonics, Grant No. DNRF147 and Center for Nanostructured Graphene, Grant No. DNRF103. N.S. acknowledges support from the Villum Foundation through Grant No. 00028233 and from the Independent Research Fund Denmark, Natural Sciences (Project No. 0135-00403B). J.I.-S. acknowledges support from the Royal Commission for the Exhibition of 1851.

[1] C. Chakraborty, L. Kinnischtzke, K. M. Goodfellow, R. Beams, and A. N. Vamivakas, Voltage-controlled quantum light from an atomically thin semiconductor, Nat. Nanotechnol. **10**, 507 (2015).

[2] Y.-M. He, G. Clark, J. R. Schaibley, Y. He, M.-C. Chen, Y.-J. Wei, X. Ding, Q. Zhang, W. Yao, X. Xu, C.-Y. Lu, and J.-W. Pan, Single quantum emitters in monolayer semiconductors, Nat. Nanotechnol. **10**, 497 (2015).

[3] M. Koperski, K. Nogajewski, A. Arora, V. Cherkez, P. Mallet, J.-Y. Veuillen, J. Marcus, P. Kossacki, and M. Potemski, Single photon emitters in exfoliated WSe_2 structures, Nat. Nanotechnol. **10**, 503 (2015).

[4] A. Srivastava, M. Sidler, A. V. Allain, D. S. Lembke, A. Kis, and A. Imamolu, Optically active quantum dots in monolayer WSe_2, Nat. Nanotechnol. **10**, 491 (2015).

[5] J. Klein, M. Lorke, M. Florian, F. Sigger, L. Sigl, S. Rey, J. Wierzbowski, J. Cerne, K. Müller, E. Mitterreiter *et al.*, Site-selectively generated photon emitters in monolayer MoS_2 via local helium ion irradiation, Nat. Commun. **10**, 2755 (2019).

[6] S. Michaelis de Vasconcellos, D. Wigger, U. Wurstbauer, A. W. Holleitner, R. Bratschitsch, and T. Kuhn, Single-photon emitters in layered van der Waals materials, Phys. Status Solidi B **259**, 2100566 (2022).

[7] M. Kianinia, Z.-Q. Xu, M. Toth, and I. Aharonovich, Quantum emitters in 2D materials: Emitter engineering, photophysics, and integration in photonic nanostructures, Appl. Phys. Rev. **9**, 011306 (2022).

[8] T. T. Tran, K. Bray, M. J. Ford, M. Toth, and I. Aharonovich, Quantum emission from hexagonal boron nitride monolayers, Nat. Nanotechnol. **11**, 37 (2016).

[9] I. Aharonovich and M. Toth, Quantum emitters in two dimensions, Science **358**, 170 (2017).

[10] M. Fischer, J. M. Caridad, A. Sajid, S. Ghaderzadeh, M. Ghorbani-Asl, L. Gammelgaard, P. Bøggild, K. S. Thygesen, A. V. Krasheninnikov, S. Xiao *et al.*, Controlled generation of luminescent centers in hexagonal boron nitride by irradiation engineering, Sci. Adv. **7**, eabe7138 (2021).

[11] N. Mendelson, D. Chugh, J. R. Reimers, T. S. Cheng, A. Gottscholl, H. Long, C. J. Mellor, A. Zettl, V. Dyakonov, P. H. Beton *et al.*, Identifying carbon as the source of visible single-photon emission from hexagonal boron nitride, Nat. Mater. **20**, 321 (2021).

[12] A. Gottscholl, M. Kianinia, V. Soltamov, S. Orlinskii, G. Mamin, C. Bradac, C. Kasper, K. Krambrock, A. Sperlich, M. Toth *et al.*, Initialization and read-out of intrinsic spin defects in a van der Waals crystal at room temperature, Nat. Mater. **19**, 540 (2020).

[13] M. Hoese, P. Reddy, A. Dietrich, M. K. Koch, K. G. Fehler, M. W. Doherty, and A. Kubanek, Mechanical decoupling of quantum emitters in hexagonal boron nitride from low-energy phonon modes, Sci. Adv. **6**, eaba6038 (2020).

[14] G. Cassabois, P. Valvin, and B. Gil, Hexagonal boron nitride is an indirect bandgap semiconductor, Nat. Photonics **10**, 262 (2016).

[15] T. T. Tran, C. Bradac, A. S. Solntsev, M. Toth, and I. Aharonovich, Suppression of spectral diffusion by anti-stokes excitation of quantum emitters in hexagonal boron nitride, Appl. Phys. Lett. **115**, 071102 (2019).

[16] K. Li, T. Smart, and Y. Ping, C_2C_N as a 2 eV single-photon emitter candidate in hexagonal boron nitride, arXiv:2110.01787.

[17] T. Vogl, R. Lecamwasam, B. C. Buchler, Y. Lu, and P. K. Lam, Compact cavity-enhanced single-photon generation with hexagonal boron nitride, ACS Photonics **6**, 1955 (2019).

[18] S. Häußler, G. Bayer, R. Waltrich, N. Mendelson, C. Li, D. Hunger, I. Aharonovich, and A. Kubanek, Tunable fiber-cavity enhanced photon emission from defect centers in hBn, Adv. Opt. Mater. **9**, 2002218 (2021).

[19] E. V. Denning, J. Iles-Smith, N. Gregersen, and J. Mork, Phonon effects in quantum dot single-photon sources, Opt. Mater. Express **10**, 222 (2020).

[20] A. Nazir and D. P. S. McCutcheon, Modelling exciton–phonon interactions in optically driven quantum dots, J. Phys.: Condens. Matter **28**, 103002 (2016).

[21] T. Q. P. Vuong, G. Cassabois, P. Valvin, A. Ouerghi, Y. Chassagneux, C. Voisin, and B. Gil, Phonon-Photon Mapping in a Color Center in Hexagonal Boron Nitride, Phys. Rev. Lett. **117**, 097402 (2016).

[22] M. A. Feldman, A. Puretzky, L. Lindsay, E. Tucker, D. P. Briggs, P. G. Evans, R. F. Haglund, and B. J. Lawrie, Phonon-induced multicolor correlations in hBn single-photon emitters, Phys. Rev. B **99**, 020101(R) (2019).

[23] P. Khatri, I. J. Luxmoore, and A. J. Ramsay, Phonon sidebands of color centers in hexagonal boron nitride, Phys. Rev. B **100**, 125305 (2019).

[24] G. Grosso, H. Moon, C. J. Ciccarino, J. Flick, N. Mendelson, L. Mennel, M. Toth, I. Aharonovich, P. Narang, and D. R. Englund, Low-temperature electronphonon interaction of quantum emitters in hexagonal boron nitride, ACS Photonics **7**, 1410 (2020).

[25] A. Sajid and K. S. Thygesen, V_NC_B defect as source of single photon emission from hexagonal boron nitride, 2D Mater. **7**, 031007 (2020).

[26] C. Jara, T. Rauch, S. Botti, M. A. L. Marques, A. Norambuena, R. Coto, J. E. Castellanos-Águila, J. R. Maze, and F. Munoz, First-principles identification of single photon emitters based on carbon clusters in hexagonal boron nitride, J. Phys. Chem. A **125**, 1325 (2021).

[27] K. Li, T. J. Smart, and Y. Ping, Carbon trimer as a 2 eV single-photon emitter candidate in hexagonal boron nitride: A first-principles study, Phys. Rev. Mater. **6**, L042201 (2022).

[28] A. Strathearn, P. Kirton, D. Kilda, J. Keeling, and B. W. Lovett, Efficient non-Markovian quantum dynamics using time-evolving matrix product operators, Nat. Commun. **9**, 3322 (2018).

[29] M. R. Jørgensen and F. A. Pollock, Exploiting the Causal Tensor Network Structure of Quantum Processes to Efficiently Simulate Non-Markovian Path Integrals, Phys. Rev. Lett. **123**, 240602 (2019).

[30] D. Gribben, A. Strathearn, J. Iles-Smith, D. Kilda, A. Nazir, B. W. Lovett, and P. Kirton, Exact quantum dynamics in structured environments, Phys. Rev. Res. **2**, 013265 (2020).

[31] D. Gribben, D. M. Rouse, J. Iles-Smith, A. Strathearn, H. Maguire, P. Kirton, A. Nazir, E. M. Gauger, and B. W. Lovett, Exact dynamics of nonadditive environments in non-Markovian open quantum systems, PRX Quantum **3**, 010321 (2022).

[32] M. K. Svendsen, Y. Kurman *et al.*, Combining density functional theory with macroscopic QED for quantum light-matter interactions in 2D materials, Nat. Commun. **12**, 2778 (2021).

[33] S. Latini, U. De Giovannini, E. J. Sie, N. Gedik, H. Hübener, and A. Rubio, Phonoritons as Hybridized Exciton-Photon-Phonon Excitations in a Monolayer *h*-BN Optical Cavity, Phys. Rev. Lett. **126**, 227401 (2021).

[34] See Supplemental Material at http://link.aps.org/supplemental/10.1103/PhysRevResearch.5.L032037 for a detailed derivation of the model, methods used, and the C_2C_N defect.

[35] A. Sajid, J. R. Reimers, and M. J. Ford, Defect states in hexagonal boron nitride: Assignments of observed properties and prediction of properties relevant to quantum computation, Phys. Rev. B **97**, 064101 (2018).

[36] This analysis is repeated in the Supplemental Material [34] for the C_2C_N defect.

[37] B. M. Garraway, Nonperturbative decay of an atomic system in a cavity, Phys. Rev. A **55**, 2290 (1997).

[38] G. Pleasance, B. M. Garraway, and F. Petruccione, Generalized theory of pseudomodes for exact descriptions of non-Markovian quantum processes, Phys. Rev. Res. **2**, 043058 (2020).

[39] E. V. Denning, J. Iles-Smith, A. D. Osterkryger, N. Gregersen, and J. Mork, Cavity-waveguide interplay in optical resonators and its role in optimal single-photon sources, Phys. Rev. B **98**, 121306(R) (2018).

[40] H. J. Carmichael, *Statistical Methods in Quantum Optics 1: Master Equations and Fokker-Planck Equations* (Springer, Berlin, 1999), Vol. 1.

[41] H. Maguire, J. Iles-Smith, and A. Nazir, Environmental Nonadditivity and Franck-Condon physics in Nonequilibrium Quantum Systems, Phys. Rev. Lett. **123**, 093601 (2019).

[42] G. D. Mahan, *Many-Particle Physics* (Springer, Berlin, 2013).

[43] F. Duschinsky, The importance of the electron spectrum in multi atomic molecules. Concerning the Franck-Condon principle, Acta Physicochim. URSS **7**, 551 (1937).

[44] R. Borrelli, A. Capobianco, and A. Peluso, Franck–Condon factors—computational approaches and recent developments, Can. J. Chem. **91**, 495 (2013).

[45] G. Kresse and J. Hafner, *Ab initio* molecular dynamics for liquid metals, Phys. Rev. B **47**, 558 (1993).

[46] H.-P. Breuer, F. Petruccione *et al.*, *The Theory of Open Quantum Systems* (Oxford University Press, Oxford, 2002).

[47] M. Popovic, M. T. Mitchison, A. Strathearn, B. W. Lovett, J. Goold, and P. R. Eastham, Quantum heat statistics with time-evolving matrix product operators, PRX Quantum **2**, 020338 (2021).

[48] G. E. Fux, E. P. Butler, P. R. Eastham, B. W. Lovett, and J. Keeling, Efficient Exploration of Hamiltonian Parameter Space for Optimal Control of Non-Markovian Open Quantum Systems, Phys. Rev. Lett. **126**, 200401 (2021).

[49] N. Makri and D. E. Makarov, Tensor propagator for iterative quantum time evolution of reduced density matrices. I. Theory, J. Chem. Phys. **102**, 4600 (1995).

[50] N. Makri and D. E. Makarov, Tensor propagator for iterative quantum time evolution of reduced density matrices. II. Numerical methodology, J. Chem. Phys. **102**, 4611 (1995).

[51] M. Cygorek, M. Cosacchi, A. Vagov, V. M. Axt, B. W. Lovett, J. Keeling, and E. M. Gauger, Simulation of open quantum systems by automated compression of arbitrary environments, Nat. Phys. **18**, 662 (2022).

[52] H. F. Trotter, On the product of semi-groups of operators, Proc. Am. Math. Soc. **10**, 545 (1959).

[53] A. Strathearn, B. W. Lovett, and P. Kirton, Efficient real-time path integrals for non-Markovian spin-boson models, New J. Phys. **19**, 093009 (2017).

[54] R. Orús, A practical introduction to tensor networks: Matrix product states and projected entangled pair states, Ann. Phys. (NY) **349**, 117 (2014).

[55] M. Ruggenthaler, N. Tancogne-Dejean, J. Flick, H. Appel, and A. Rubio, From a quantum-electrodynamical light–matter description to novel spectroscopies, Nat. Rev. Chem. **2**, 0118 (2018).

[56] J. Flick, D. M. Welakuh, M. Ruggenthaler, H. Appel, and A. Rubio, Light–matter response in nonrelativistic quantum electrodynamics, ACS Photonics **6**, 2757 (2019).

[57] S. Mukamel, *Principles of Nonlinear Optical Spectroscopy* (Oxford University Press, Oxford, 1999).

[58] J. Iles-Smith, D. P. S. McCutcheon, A. Nazir, and J. Mørk, Phonon scattering inhibits simultaneous near-unity efficiency and indistinguishability in semiconductor single-photon sources, Nat. Photonics **11**, 521 (2017).

[59] J. Del Pino, F. A. Y. N. Schröder, A. W. Chin, J. Feist, and F. J. Garcia-Vidal, Tensor Network Simulation of Non-Markovian Dynamics in Organic Polaritons, Phys. Rev. Lett. **121**, 227401 (2018).

[60] S. White, C. Stewart, A. S. Solntsev, C. Li, M. Toth, M. Kianinia, and I. Aharonovich, Phonon dephasing and spectral diffusion of quantum emitters in hexagonal boron nitride, Optica **8**, 1153 (2021).